INSTITUTE OF PHYSICS PUBLISHING INVERSE PROBLEMS

Inverse Problems **17** (2001) 1357–1371 PII: S0266-5611(01)20858-2

Image reconstruction in 2D SPECT with 180° acquisition

Frédéric Noo[1,2,3] **and Jean-Marc Wagner**[1]

[1] Institut d'Electricité Montefiore, Université de Liège, Belgium
[2] Department of Radiology, University of Utah, USA

E-mail: noo@doug.med.utah.edu

Received 12 January 2001, in final form 2 May 2001
Published 30 August 2001
Online at stacks.iop.org/IP/17/1357

Abstract

This work concerns 2D SPECT imaging with uniform attenuation in the activity region. In this paper, it is shown that exact and stable reconstruction does not require the data to be known over 360° as has been previously assumed. An angular range of 180° is sufficient in parallel-beam geometry. A reconstruction formula which uses only data on a half-turn is provided with implementation details. Simulations are performed to support the mathematical result.

1. Introduction

This work concerns two-dimensional (2D) image reconstruction in single photon emission computed tomography (SPECT) using parallel-beam collimators.

The objective of 2D SPECT imaging is to visualize the concentration of a radioactive tracer within the slice of a 3D body. To achieve this goal, the number of photons emitted along different directions within the slice is measured to obtain information on the activity distribution. In this study, these measurements are described using the line-integral model of the attenuated Radon transform. Any deviation from that model due to physical effects such as Poisson noise, scattering, or detector response, is viewed as a source of data noise. The 2D image to be reconstructed is either denoted as f, $f(\underline{x})$ or $f(x, y)$, with $\underline{x} = (x, y)$. It is assumed that f is bounded and compactly supported in

$$\Omega = \{\underline{x} \in \mathbb{R}^2 \mid \quad |\underline{x}| < D\} \tag{1}$$

where D is the radius of the activity region. The attenuated Radon transform of f is

$$p(\phi, s) = \int_{-\infty}^{+\infty} \mathrm{d}t\, f(s\underline{\theta} + t\underline{\theta}^{\perp}) \exp\left(- \int_{t}^{+\infty} \mathrm{d}l\, \mu(s\underline{\theta} + l\underline{\theta}^{\perp}) \right). \tag{2}$$

[3] Corresponding address: University of Utah, Department of Radiology, CAMT Building, 729 Arapeen Drive, Salt Lake City, Utah 84108, USA.

0266-5611/01/051357+15$30.00

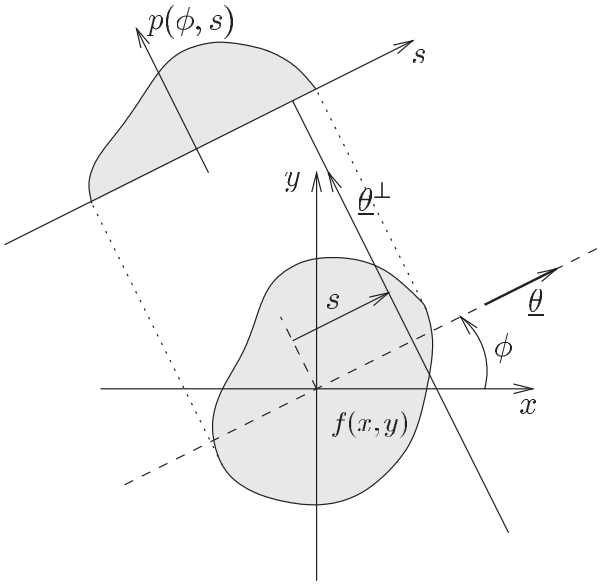

Figure 1. Illustration of different parameters appearing in the definition of the attenuated Radon transform.

See figure 1 for an illustration of the different variables appearing in this expression. By definition, $\underline{\theta} = (\cos\phi, \sin\phi)$ and $\underline{\theta}^{\perp} = (-\sin\phi, \cos\phi)$. The function $\mu(\underline{x})$ describes the way the photons are attenuated along the measurement lines defined by s and ϕ; it is referred to as the attenuation map of the body under investigation and is considered to be known. For a fixed ϕ, the set of values $p(\phi, s)$ obtained by varying s in $\mathbb{R}$ is called attenuated projection of f.

Recently, exact formulae have been derived and implemented for the inversion of (2) with $p(\phi, s)$ known for $\phi \in [0, 2\pi)$ and $s \in \mathbb{R}$ see [1–3]. In this paper, we are interested in the reconstruction of f from projections which are acquired over a range of 180° instead of 360°. In the case of no attenuation, i.e. when $\mu(\underline{x}) = 0$, it is well known that an angular range of 180° is sufficient to determine f in a unique and stable way. On the other hand, when $\mu(\underline{x}) \neq 0$, it is generally believed that the data $p(\phi, s)$ must be known over 360°. The contribution of this paper is to show that this statement is wrong. More specifically, it is shown that exact and stable reconstruction of f can be achieved using only measurements on a half-turn.

The practical implications of this work are important. By reducing the data acquisition from 360° to 180°, the data acquisition time can be halfed, thereby increasing patient throughput and making the exam less uncomfortable for the patient. Another advantage is the possibility to disregard projections which undergo high attenuation such as those traversing the spine in thorax imaging. These projections are usually very noisy and tend to limit the image quality.

A simplification of the relation (2) between the data p and the image f occurs when the activity is contained in a convex region where μ is constant. It will be assumed that this condition holds. In this case, the data $p(\phi, s)$ can be modified into

$$g_0(\phi, s) = \int_{\mathbb{R}} \mathrm{d}t \; f(s\,\underline{\theta} + t\,\underline{\theta}^{\perp})\,\mathrm{e}^{\mu_0 t} \tag{3}$$

where μ_0 is the value of μ in the activity region (i.e. in the support of f). Occasionally, we will use the notation $\overline{\mu}_0 = \mu_0/2\pi$. In the literature, g_0 is referred to as the exponential Radon

transform of f and $g_0(\phi, \cdot)$ is called an exponential parallel-beam projection of f. The relation between p and g_0 can be written in the form

$$g_0(\phi, s) = p(\phi, s)\, m_\mu(\phi, s) \tag{4}$$

where $m_\mu(\phi, s)$ is calculated from the attenuation map. See [4] for details.

Numerous papers have been written on the inversion of the exponential Radon transform with constant attenuation. See [5–22] for the most representative works. All these references suppose that $g_0(\phi, s)$ is known for all angles $\phi \in [0, 2\pi)$. In this paper, it is assumed that $g_0(\phi, s)$ is only known for $\phi \in [0, \pi)$. To our knowledge, no mathematical results exist about inversion from this limited data set. It has been observed in practice that iterative reconstruction methods such as the expectation-maximization algorithm can provide accurate results from 180° data. However, no convergence theorems support these observations.

Conceptually, recovering f from $g_0(\phi, s)$ with $\phi \in [0, \pi)$ is equivalent to reconstructing f from

$$g(\phi, s) = \int_{\mathbb{R}} \mathrm{d}t \;\; f(s\,\underline{\theta} + t\,\underline{\theta}^{\perp})\, \mathrm{e}^{\mu(\phi)\, t} \tag{5}$$

with $\phi \in [0, 2\pi)$, $s \in \mathbb{R}$ and

$$\mu(\phi) = \begin{cases} \mu_0 & \text{if} \quad \phi \in [0, \pi) \\ -\mu_0 & \text{if} \quad \phi \in [\pi, 2\pi). \end{cases} \tag{6}$$

With this definition of $\mu(\phi)$,

$$g(\phi, s) = \begin{cases} g_0(\phi, s) & \text{if} \quad \phi \in [0, \pi), \qquad s \in \mathbb{R} \\ g_0(\phi - \pi, -s) & \text{if} \quad \phi \in [\pi, 2\pi), \qquad s \in \mathbb{R}. \end{cases} \tag{7}$$

Thus, $g_0(\phi, s)$ is indeed only required for $\phi \in [0, \pi)$.

The transform $g(\phi, s)$ of equation (5) is referred to as the exponential Radon transform with angle dependent attenuation factor. This transform has been investigated by Hazou and Solmon [13], Kuchment and Schneiberg [23], and Palamodov [24]. Hazou and Solmon have obtained some existence results. Kuchment and Schneiberg have derived an inversion formula of the filtered-backprojection type. The proof assumed that $\mu(\phi)$ is positive and continuously differentiable. Palamodov has derived the formula of Kuchment and Schneiberg for $\mu(\phi)$ of arbitrary sign but such that $\mu(\phi + \pi) = \mu(\phi)$. None of these results applies directly to the inversion of (5) with $\mu(\phi)$ given by equation (6).

This paper presents a formula for the reconstruction of f from $g_0(\phi, s)$ with $\phi \in [0, \pi)$. This formula is derived in two steps. First, a Fredholm integral equation of the second type is derived for f. Section 2 presents the details of this derivation. Next, the integral equation is solved. It is shown in section 3 that a stable solution can be obtained in the form of a Neumann series. Section 4 discusses implementation details and presents simulation results. Conclusions are given with a short discussion in section 5.

2. An integral equation for f

Let the symbol $*$ denote the convolution operation in $\mathbb{R}^2$. In this section, it is shown that f is the limit in L^2 of the sequence $f_n = u_n + w_n * f$ where

$$u_n(\underline{x}) = \int_0^{\pi} \mathrm{d}\phi\, \mathrm{e}^{-\mu_0 \underline{x}\cdot\underline{\theta}^{\perp}} \int_{\overline{\mu}_0 \leqslant |\sigma| \leqslant \sqrt{n^2 + \overline{\mu}_0^2}} \mathrm{d}\sigma\, |\sigma|\, \mathrm{e}^{\mathrm{i}\, 2\pi\, \sigma \underline{x}\cdot\underline{\theta}}\, \mathcal{F} g_0(\phi, \sigma) \tag{8}$$

and

$$w_n(x, y) = \int_{-1}^{1} \mathrm{d}p\, \mathrm{e}^{\mu_0 p y} \int_{\overline{\mu}_0 |p| \leqslant |\sigma| \leqslant \sqrt{n^2 + \overline{\mu}_0^2 p^2}} \mathrm{d}\sigma\, \mathrm{i}\, \overline{\mu}_0\, \mathrm{sign}(\sigma)\, \mathrm{e}^{\mathrm{i}\, 2\pi\, x\sigma}. \tag{9}$$

Formally, we write

$$f = u_\infty + w_\infty * f \tag{10}$$

with

$$u_\infty(\underline{x}) = \int_0^\pi \mathrm{d}\phi\, \mathrm{e}^{-\mu_0 \underline{x}\cdot\underline{\theta}^\perp} \int_{|\sigma| \geqslant \overline{\mu}_0} \mathrm{d}\sigma\, |\sigma|\, \mathrm{e}^{\mathrm{i}\, 2\pi\, \sigma \underline{x}\cdot\underline{\theta}}\, \mathcal{F}g_0(\phi, \sigma) \tag{11}$$

and

$$\begin{aligned} w_\infty(x, y) &= \int_{-1}^{1} \mathrm{d}p\, \mathrm{e}^{\mu_0 p y} \int_{|\sigma| \geqslant \overline{\mu}_0 |p|} \mathrm{d}\sigma\, \mathrm{i}\, \overline{\mu}_0\, \mathrm{sign}(\sigma)\, \mathrm{e}^{\mathrm{i}\, 2\pi\, x\sigma} \\ &= \frac{\overline{\mu}_0}{\pi\, x} \left\{ \frac{\sinh \mu_0(y + \mathrm{i}x)}{\mu_0(y + \mathrm{i}x)} + \frac{\sinh \mu_0(y - \mathrm{i}x)}{\mu_0(y - \mathrm{i}x)} \right\}. \end{aligned} \tag{12}$$

Note that u_∞ is the result of applying the filtered-backprojection reconstruction formula of Tretiak and Metz [6] to the available projections.

The derivation of (10) is based on the central slice theorem for $g(\phi, s)$ (equation (5)) with $\mu(\phi)$ given by equation (6):

$$\mathcal{F}g(\phi, \sigma) = \mathcal{F}f(\sigma\underline{\theta} + \mathrm{i}\, \overline{\mu}(\phi)\, \underline{\theta}^\perp). \tag{13}$$

In this equation, $\mathcal{F}g(\phi, \sigma)$ is the 1D Fourier transform of $g(\phi, s)$ w.r.t. s and $\mathcal{F}f$ is the analytic continuation of the Fourier transform of f. The proof of (13) can be found in [13]. As in [11], we introduce two functions $\omega(\phi, \sigma)$ and $\alpha(\phi, \sigma)$ such that

$$\sigma = \omega\, \cos\alpha, \qquad \mathrm{i}\, \overline{\mu}(\phi) = \omega\, \sin\alpha. \tag{14}$$

For $|\sigma| > |\overline{\mu}(\phi)|$,

$$\omega = \sqrt{\sigma^2 - \overline{\mu}^2(\phi)}, \qquad \tan\alpha = \mathrm{i}\, \overline{\mu}(\phi)/\sigma. \tag{15}$$

With the definition of $\underline{\theta}$ and $\underline{\theta}^\perp$, it is easy to see that

$$\sigma\underline{\theta} + \mathrm{i}\, \overline{\mu}(\phi)\, \underline{\theta}^\perp = (\omega\, \cos(\phi + \alpha), \omega\, \sin(\phi + \alpha)). \tag{16}$$

Thus,

$$\mathcal{F}g(\phi, \sigma) = \mathcal{F}f(\omega\, \cos(\phi + \alpha), \omega\, \sin(\phi + \alpha)). \tag{17}$$

Now, f is expressed as the inverse of its Fourier transform in $L^2(\mathbb{R}^2)$, using polar coordinates:

$$f(x, y) = \lim_{n \to \infty} f_n(x, y) \tag{18}$$

with

$$f_n(x, y) = \int_0^n \mathrm{d}\hat{\omega}\, \hat{\omega} \int_0^{2\pi} \mathrm{d}\phi\, \mathrm{e}^{\mathrm{i}\, 2\pi\, \hat{\omega}(x\, \cos\phi + y\, \sin\phi)}\, \mathcal{F}f(\hat{\omega}\, \cos\phi, \hat{\omega}\, \sin\phi). \tag{19}$$

The limit holds in $L^2(\mathbb{R}^2)$. Let $z = \phi + \mathrm{i}\tau$ and $C_0 = \{z \in \mathbb{C} \mid\ \phi \in [0, 2\pi),\ \tau = 0\}$. The inner integral in equation (19) is viewed as an integral along the curve C_0 in the complex domain of z. That is,

$$\begin{aligned} &\int_0^{2\pi} \mathrm{d}\phi\, \mathrm{e}^{\mathrm{i}\, 2\pi\, \hat{\omega}(x\, \cos\phi + y\, \sin\phi)}\, \mathcal{F}f(\hat{\omega}\, \cos\phi, \hat{\omega}\, \sin\phi) \\ &\qquad = \int_{C_0} \mathrm{d}z\, \mathrm{e}^{\mathrm{i}\, 2\pi\, \hat{\omega}(x\, \cos z + y\, \sin z)}\, \mathcal{F}f(\hat{\omega}\, \cos z, \hat{\omega}\, \sin z). \end{aligned} \tag{20}$$

Since f is bounded and compactly supported, $\mathcal{F}f(\hat{\omega}\cos z, \hat{\omega}\sin z)$ is an entire analytic function of z. Therefore, the integration theorem of Cauchy can be applied to obtain

$$\int_0^{2\pi} \mathrm{d}\phi\, \mathrm{e}^{\mathrm{i}\,2\pi\,\hat{\omega}(x\,\cos\phi + y\,\sin\phi)}\,\mathcal{F}f(\hat{\omega}\,\cos\phi, \hat{\omega}\,\sin\phi)$$
$$= \sum_{l=1}^{5} \int_{C_l} \mathrm{d}z\, \mathrm{e}^{\mathrm{i}\,2\pi\,\hat{\omega}(x\,\cos z + y\,\sin z)}\,\mathcal{F}f(\hat{\omega}\,\cos z, \hat{\omega}\,\sin z) \tag{21}$$

where the curves C_l form a bounded domain with C_0. See figure 1 for an illustration of these curves. In this figure, $\hat{\alpha}(\hat{\omega})$ is such that

$$\tan\hat{\alpha}(\hat{\omega}) = \frac{\mathrm{i}\,\overline{\mu}_0}{\sqrt{\hat{\omega}^2 + \overline{\mu}^2(\phi)}}. \tag{22}$$

The use of formula (21) in the expression of $f_n(x, y)$ yields

$$f_n(x, y) = f_n^{(1)}(x, y) + f_n^{(2)}(x, y) \tag{23}$$

where $f_n^{(1)}(x, y)$ is the contribution from the curves C_2 and C_4, and $f_n^{(2)}(x, y)$ is the contribution from C_1, C_3 and C_5.

The expression of $f_n^{(1)}(x, y)$ is first developed. By definition of C_2 and C_4,

$$f_n^{(1)}(x, y) = \int_0^n \mathrm{d}\hat{\omega}\,\hat{\omega} \int_0^{\pi} \mathrm{d}\phi\, \mathrm{e}^{\mathrm{i}\,2\pi\,\hat{\omega}(x\cos(\phi+\hat{\alpha}) + y\sin(\phi+\hat{\alpha}))}\mathcal{F}f(\hat{\omega}\cos(\phi+\hat{\alpha}), \hat{\omega}\sin(\phi+\hat{\alpha}))$$
$$+ \int_0^n \mathrm{d}\hat{\omega}\,\hat{\omega} \int_{\pi}^{2\pi} \mathrm{d}\phi\, \mathrm{e}^{\mathrm{i}\,2\pi\,\hat{\omega}(x\cos(\phi-\hat{\alpha}) + y\sin(\phi-\hat{\alpha}))}\mathcal{F}(\hat{\omega}\cos(\phi-\hat{\alpha}), \hat{\omega}\sin(\phi-\hat{\alpha})). \tag{24}$$

Considering $\phi \in [0, 2\pi)$ as a fixed parameter, we apply the change of variable

$$\hat{\omega} = \sqrt{\sigma^2 - \overline{\mu}^2(\phi)}, \qquad \sigma \geqslant \overline{\mu}_0. \tag{25}$$

This change of variable is such that

$$\sigma\,\mathrm{d}\sigma = \hat{\omega}\,\mathrm{d}\hat{\omega}, \qquad \hat{\omega} = \omega(\phi, \sigma) \qquad \text{and} \qquad \hat{\alpha}(\hat{\omega}) = \begin{cases} \alpha(\phi, \sigma) & \text{if} \quad \phi \in [0, \pi) \\ -\alpha(\phi, \sigma) & \text{if} \quad \phi \in [\pi, 2\pi) \end{cases} \tag{26}$$

where $\alpha(\phi, \sigma)$ and $\omega(\phi, \sigma)$ are the functions introduced in (14) and (15). Using (25) with the central slice theorem (equations (16) and (17)) leads to

$$f_n^{(1)}(x, y) = \int_0^{\pi} \mathrm{d}\phi \int_{\overline{\mu}_0}^{\sqrt{n^2+\overline{\mu}_0^2}} \mathrm{d}\sigma\,\sigma\, \mathrm{e}^{\mathrm{i}\,2\pi\,\underline{x}\cdot(\sigma\,\underline{\theta} + \mathrm{i}\,\overline{\mu}(\phi)\,\underline{\theta}^{\perp})}\,\mathcal{F}g(\phi, \sigma)$$
$$+ \int_{\pi}^{2\pi} \mathrm{d}\phi \int_{\overline{\mu}_0}^{\sqrt{n^2+\overline{\mu}_0^2}} \mathrm{d}\sigma\,\sigma\, \mathrm{e}^{\mathrm{i}\,2\pi\,\underline{x}\cdot(\sigma\,\underline{\theta} + \mathrm{i}\,\overline{\mu}(\phi)\,\underline{\theta}^{\perp})}\,\mathcal{F}g(\phi, \sigma). \tag{27}$$

That is,

$$f_n^{(1)}(x, y) = \int_0^{\pi} \mathrm{d}\phi\, \mathrm{e}^{-\mu_0\underline{x}\cdot\underline{\theta}^{\perp}} \int_{\overline{\mu}_0}^{\sqrt{n^2+\overline{\mu}_0^2}} \mathrm{d}\sigma\,\sigma\, \mathrm{e}^{\mathrm{i}\,2\pi\,\sigma\underline{x}\cdot\underline{\theta}}\,\mathcal{F}g(\phi, \sigma)$$
$$+ \int_{\pi}^{2\pi} \mathrm{d}\phi\, \mathrm{e}^{\mu_0\underline{x}\cdot\underline{\theta}^{\perp}} \int_{\overline{\mu}_0}^{\sqrt{n^2+\overline{\mu}_0^2}} \mathrm{d}\sigma\,\sigma\, \mathrm{e}^{\mathrm{i}\,2\pi\,\sigma\underline{x}\cdot\underline{\theta}}\,\mathcal{F}g(\phi, \sigma). \tag{28}$$

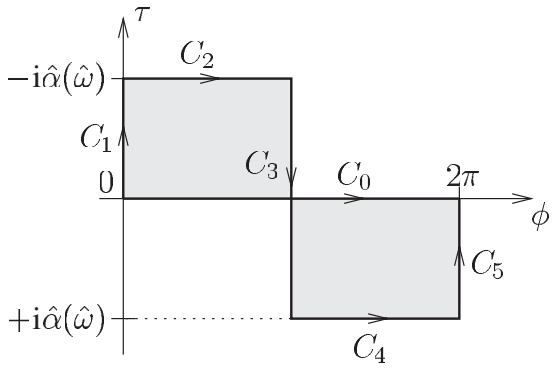

Figure 2. Definition of contours C_l, $l = 1, \ldots, 5$ forming a bounded domain with the curve C_0 in formula (20). These contours are used in formula (21) according to Cauchy's integration theorem. The function $\hat{\alpha}(\hat{\omega})$ is defined in equation (22).

Recall from equation (7) that $g(\phi, s) = g(\phi - \pi, -s)$ for $\phi \in [\pi, 2\pi)$. This relation implies $\mathcal{F}g(\phi, \sigma) = \mathcal{F}g(\phi - \pi, -\sigma)$ for $\phi \in [\pi, 2\pi)$. The change of variable $\phi' = \phi - \pi$, $\sigma' = -\sigma$ followed by a substitution of ϕ' into ϕ and s' into s in the second integral of (28) gives

$$f_n^{(1)}(x, y) = \int_0^{\pi} \mathrm{d}\phi\, \mathrm{e}^{-\mu_0 \underline{x}\cdot\underline{\theta}^{\perp}} \int_{\overline{\mu}_0}^{\sqrt{n^2+\overline{\mu}_0^2}} \mathrm{d}\sigma\, \sigma\, \mathrm{e}^{\mathrm{i}\,2\pi\,\sigma \underline{x}\cdot\underline{\theta}}\, \mathcal{F}g(\phi, \sigma)$$
$$+ \int_0^{\pi} \mathrm{d}\phi\, \mathrm{e}^{-\mu_0 \underline{x}\cdot\underline{\theta}^{\perp}} \int_{-\sqrt{n^2+\overline{\mu}_0^2}}^{-\overline{\mu}_0} \mathrm{d}\sigma\, (-\sigma)\, \mathrm{e}^{\mathrm{i}\,2\pi\,\sigma \underline{x}\cdot\underline{\theta}}\, \mathcal{F}g(\phi, \sigma). \tag{29}$$

Therefore,

$$f_n^{(1)}(x, y) = \int_0^{\pi} \mathrm{d}\phi\, \mathrm{e}^{-\mu_0 \underline{x}\cdot\underline{\theta}^{\perp}} \int_{\overline{\mu}_0 \leqslant |\sigma| \leqslant \sqrt{n^2+\overline{\mu}_0^2}} \mathrm{d}\sigma\, |\sigma|\, \mathrm{e}^{\mathrm{i}\,2\pi\,\sigma \underline{x}\cdot\underline{\theta}}\, \mathcal{F}g(\phi, \sigma). \tag{30}$$

Since $g(\phi, s) = g_0(\phi, s)$ for $\phi \in [0, \pi)$, we see that $f_n^{(1)}$ is identical to the function u_n used to define u_∞ in equation (10).

Now, the expression of the term $f_n^{(2)}(x, y)$ in (23) is developed. By definition of C_1, C_3 and C_5 (see figure 2),

$$f_n^{(2)}(x, y) = \mathrm{i} \int_0^{n} \mathrm{d}\hat{\omega}\, \hat{\omega} \int_0^{-\mathrm{i}\,\hat{\alpha}(\hat{\omega})} \mathrm{d}\tau\, \mathrm{e}^{\mathrm{i}\,2\pi\,\hat{\omega}(x\cos\mathrm{i}\tau + y\sin\mathrm{i}\tau)}\, \mathcal{F}f(\hat{\omega}\cos\mathrm{i}\tau, \hat{\omega}\sin\mathrm{i}\tau)$$
$$-\mathrm{i} \int_0^{n} \mathrm{d}\hat{\omega}\, \hat{\omega} \int_{\mathrm{i}\,\hat{\alpha}(\hat{\omega})}^{-\mathrm{i}\,\hat{\alpha}(\hat{\omega})} \mathrm{d}\tau\, \mathrm{e}^{-\mathrm{i}\,2\pi\,\hat{\omega}(x\cos\mathrm{i}\tau + y\sin\mathrm{i}\tau)}\, \mathcal{F}f(-\hat{\omega}\cos\mathrm{i}\tau, -\hat{\omega}\sin\mathrm{i}\tau)$$
$$+\mathrm{i} \int_0^{n} \mathrm{d}\hat{\omega}\, \hat{\omega} \int_{\mathrm{i}\,\hat{\alpha}(\hat{\omega})}^{0} \mathrm{d}\tau\, \mathrm{e}^{\mathrm{i}\,2\pi\,\hat{\omega}(x\cos\mathrm{i}\tau + y\sin\mathrm{i}\tau)}\, \mathcal{F}f(\hat{\omega}\cos\mathrm{i}\tau, \hat{\omega}\sin\mathrm{i}\tau). \tag{31}$$

That is,

$$f_n^{(2)}(x, y) = \mathrm{i} \int_{-n}^{n} \mathrm{d}\hat{\omega}\, \hat{\omega} \int_{\mathrm{i}\,\hat{\alpha}(\hat{\omega})}^{-\mathrm{i}\,\hat{\alpha}(\hat{\omega})} \mathrm{d}\tau\, \mathrm{e}^{\mathrm{i}\,2\pi\,\hat{\omega}(x\cos\mathrm{i}\tau + y\sin\mathrm{i}\tau)}\, \mathcal{F}f(\hat{\omega}\cos\mathrm{i}\tau, \hat{\omega}\sin\mathrm{i}\tau) \tag{32}$$

since $\hat{\alpha}(-\hat{\omega}) = \hat{\alpha}(\hat{\omega})$ (see equation (22)). Using the definition of the Fourier tranform of $f(x, y)$, this equation becomes

$$f_n^{(2)}(x, y) = \int_{\mathbb{R}^2} \mathrm{d}x'\, \mathrm{d}y'\, f(x', y')\, h_n(x - x', y - y') \tag{33}$$

with

$$h_n(x, y) = \mathrm{i} \int_{-n}^{n} \mathrm{d}\hat{\omega}\, \hat{\omega} \int_{\mathrm{i}\,\hat{\alpha}(\hat{\omega})}^{-\mathrm{i}\,\hat{\alpha}(\hat{\omega})} \mathrm{d}\tau\, \mathrm{e}^{\mathrm{i}\,2\pi\,\hat{\omega}(x\cos\mathrm{i}\tau + y\sin\mathrm{i}\tau)}. \tag{34}$$

The expression of h_n can be simplified as follows. First, apply the change of variable

$$\tan\mathrm{i}\tau = -\frac{\mathrm{i}\,\overline{\mu}_0\, p\,\mathrm{sign}(\hat{\omega})}{\sqrt{\hat{\omega}^2 + \overline{\mu}_0^2\, p^2}}, \qquad \cos\mathrm{i}\tau = \frac{\sqrt{\hat{\omega}^2 + \overline{\mu}_0^2\, p^2}}{|\hat{\omega}|}, \qquad \sin\mathrm{i}\tau = -\frac{\mathrm{i}\overline{\mu}_0\, p}{\hat{\omega}}, \tag{35}$$

with $\hat{\omega}$ fixed. This yields

$$h_n(x, y) = \int_{-n}^{n} \mathrm{d}\hat{\omega}\, \hat{\omega} \int_{-1}^{1} \mathrm{d}p\, \frac{\mathrm{i}\overline{\mu}_0}{\sqrt{\hat{\omega}^2 + \overline{\mu}_0^2\, p^2}}\, \mathrm{e}^{\mu_0 py}\, \mathrm{e}^{\mathrm{i}\,2\pi\, x\,\mathrm{sign}(\hat{\omega})\sqrt{\hat{\omega}^2 + \overline{\mu}_0^2\, p^2}}. \tag{36}$$

Next, apply the change of variable

$$\sigma^2 = \hat{\omega}^2 + \overline{\mu}_0^2\, p^2, \qquad \mathrm{sign}(\sigma) = \mathrm{sign}(\hat{\omega}) \tag{37}$$

with p fixed. The result is

$$h_n(x, y) = \int_{-1}^{1} \mathrm{d}p\, \mathrm{e}^{\mu_0 py} \int_{\overline{\mu}_0 |p| \leqslant |\sigma| \leqslant \sqrt{n^2 + \overline{\mu}_0^2\, p^2}} \mathrm{d}\sigma\, \mathrm{i}\,\overline{\mu}_0\, \mathrm{sign}(\sigma)\, \mathrm{e}^{\mathrm{i}\,2\pi\, x\sigma}. \tag{38}$$

We see that h_n is equal to the function w_n of equation (9). Therefore, $f_n^{(2)}$ is identical to the function $w_n * f$ used to define $w_\infty * f$ in equation (10).

In summary, we have shown that f is the limit in $L^2(\mathbb{R}^2)$ of the sequence

$$\begin{aligned} f_n &= f_n^{(1)} + f_n^{(2)} \\ &= u_n + w_n * f \end{aligned} \tag{39}$$

with u_n and w_n given by equations (8) and (9), respectively. To derive this result, it was assumed that f is bounded and compactly supported in Ω.

3. A reconstruction formula

Let $\chi(\underline{x})$ be the characteristic function of the set Ω. Since f is compactly supported in Ω, $f = \chi\, f$. Thus, f can be seen as the limit in $L^2(\Omega)$ of the sequence $f_n = \chi\, u_n + \chi\, (w_n * \chi\, f)$. In the appendix, we show that the sequence $\chi\, (w_n * \chi\, \psi)$ converges in $L^2(\Omega)$ for any function $\psi \in L^2(\Omega)$. This result authorizes us to introduce a linear operator $K : L^2(\Omega) \to L^2(\Omega)$ such that

$$K\psi = \lim_{n\to\infty} \chi\, (w_n * \chi\, \psi), \qquad \psi \in L^2(\Omega), \tag{40}$$

where the limit holds in $L^2(\Omega)$. In particular, we have

$$f = \chi\, u_\infty + Kf. \tag{41}$$

Hereafter, it is shown that the above integral equation admits a unique and stable solution in $L^2(\Omega)$. Moreover, this solution can be written in the form of a Neumann series. The idea of introducing $\chi(\underline{x})$ was suggested by the work of Palamodov [24].

First, note that $w_n(x, y)$ is an odd function, i.e. $w_n(-x, -y) = -w_n(x, y)$. This relation is easily deduced from equation (9). Next, let $K_n\psi = \chi\, (w_n * \chi\, \psi)$. Since w_n is odd, the scalar product

$$(K_n\psi_1, \psi_2) = -(\psi_1, K_n\psi_2) \tag{42}$$

for any functions ψ_1 and ψ_2 in $L_2(\Omega)$. Therefore,

$$(K\psi_1, \psi_2) = -(\psi_1, K\psi_2) \tag{43}$$

for any ψ_1 and ψ_2 in $L^2(\Omega)$ because $K_n\psi$ converges strongly to $K\psi$ for $\psi \in L^2(\Omega)$ (i.e. $\|K_n\psi - K\psi\| \to 0$). Equation (43) shows that K is antisymmetric. Since this equation is valid for any functions ψ_1 and ψ_2 in $L^2(\Omega)$ and K is a linear operator, we deduce from the theorem of Hellingter–Toeplitz[4] that K is bounded and $(-K)$ is the adjoint operator of K (see chapter 10.1 in [25] for more details).

The discussion is now focused on solving equation (41) for f. Suppose first that $\|K\| < 1$. (Such an assumption can be made since K is bounded.) In such a case, equation (41) can be applied recursively to obtain

$$\begin{aligned} f &= \chi\ u_\infty + Kf \\ &= \chi\ u_\infty + K(\chi\ u_\infty + Kf) \\ &= \chi\ u_\infty + K\ \chi\ u_\infty + K^2\ (\chi\ u_\infty + Kf) \\ &= \sum_{n=0}^{\infty} K^n \chi\ u_\infty. \end{aligned} \tag{44}$$

This series converges in $L^2(\Omega)$ and is such that

$$\|f\| < \frac{\|\chi\ u_\infty\|}{1 - \|K\|}. \tag{45}$$

When $\|K\| < 1$, we see thus that (41) admits a unique solution in $L^2(\Omega)$. This solution is stable because $\chi\ u_\infty$ is continuous as a linear functional of g_0. However, the condition $\|K\| < 1$ is not automatically satisfied. Formally, $K\psi = \chi\ (w_\infty * \chi\ \psi)$ with w_∞ given by equation (12). Therefore, the condition $\|K\| < 1$ can only be satisfied for small values of $\mu_0 D$ where D is the radius of Ω. To ensure the convergence of the series in (44) for a given μ_0, fixed by physical constraints, the activity f must thus be confined to a sufficiently small region. The computer experiment carried out in section 4 shows that this condition is actually too restrictive for practical applications.

To overcome the restriction $\|K\| < 1$, we introduce a relaxation factor $\gamma \in (0, 1]$ in equation (41) such that

$$f = \gamma\ \chi\ u_\infty + ((1 - \gamma)\ I + \gamma\ K)\ f \tag{46}$$

where I is the identity operator. This equation is rewritten in the form

$$f = \gamma\ \chi\ u_\infty + \hat{K} f \tag{47}$$

where $\hat{K} = (1 - \gamma)\ I + \gamma\ K$. We show below that γ can be chosen so that $\|\hat{K}\| < 1$ for any value of $\mu_0 D$. This property is a direct consequence of the antisymmetry of K. By definition,

$$\begin{aligned} \|\hat{K}\psi\|^2 &= (\hat{K}\psi, \hat{K}\psi) \\ &= \big((1 - \gamma)\ \psi + \gamma\ K\psi, (1 - \gamma)\ \psi + \gamma\ K\psi\big) \\ &= (1 - \gamma)^2\ \|\psi\|^2 + \gamma^2\ \|K\psi\|^2 + \gamma\ (1 - \gamma)\ (\psi, K\psi) + \gamma\ (1 - \gamma)\ (K\psi, \psi) \\ &= (1 - \gamma)^2\ \|\psi\|^2 + \gamma^2\ \|K\psi\|^2 \end{aligned} \tag{48}$$

for any $\psi \in L^2(\Omega)$ since $(K\psi, \psi) = -(\psi, K\psi)$. Hence,

$$\|\hat{K}\|^2 = (1 - \gamma)^2 + \gamma^2\ \|K\|^2. \tag{49}$$

[4] The theorem of Hellingter–Toeplitz can be stated as follows [25]: let K_1 and K_2 be two linear operators, each defined on all of a complex Hilbert space H. If $(K_1\psi_1, \psi_2) = (\psi_1, K_2\psi_2)$ for all $\psi_1, \psi_2 \in H$ then K_1 is bounded and K_2 is its Hilbert-adjoint operator.

From this result, we see that the norm of $\hat{K}$ admits a minimum at

$$\gamma = \gamma_{\text{opt}} = \frac{1}{1 + \|K\|^2}. \tag{50}$$

Let $\hat{K}_{\text{opt}} = (1 - \gamma_{\text{opt}})\, I + \gamma_{\text{opt}}\, K$ be the value of $\hat{K}$ at this minimum. We have

$$\|\hat{K}_{\text{opt}}\| = \frac{\|K\|}{\left(1 + \|K\|^2\right)^{1/2}}. \tag{51}$$

Therefore, by selecting $\gamma = \gamma_{\text{opt}}$ in (46), the integral equation (41) is modified into

$$f = \gamma_{\text{opt}}\, \chi\, u_\infty + \hat{K}_{\text{opt}} f \tag{52}$$

with $\|\hat{K}_{\text{opt}}\| < 1$. Taking on the same recursive approach as in equation (44), we obtain

$$f = \gamma_{\text{opt}} \sum_{n=0}^{\infty} (\hat{K}_{\text{opt}})^n\, \chi\, u_\infty, \tag{53}$$

where the series converges in $L^2(\Omega)$ for any value of $\mu_0 D$.

Equation (53) defines a unique and stable solution to the integral equation (41). For this solution, we have

$$\|f\| < \frac{\gamma_{\text{opt}}\, \|\chi\, u_\infty\|}{1 - \|\hat{K}_{\text{opt}}\|}. \tag{54}$$

4. Implementation details and simulations

The reconstruction of f from formula (53) can be implemented in the following way:

- *Step 1.* Compute $f_0 = \chi\, u_\infty$ from the available projections g_0. See formula (11).
- *Step 2.* Compute $f_n = \hat{K}_{\text{opt}} f_{n-1} = (1 - \gamma_{\text{opt}})\, f_{n-1} + \gamma_{\text{opt}}\, K f_{n-1}$ for $n = 1, \ldots, N$, with γ_{opt} given by equation (50).
- *Step 3.* Compute $f_N \simeq \gamma_{\text{opt}} \sum_{n=0}^{N} f_n$.

The function f_N represents the reconstructed image. The accuracy $\|f_N - f\|$ of the reconstruction depends on $\|K\|$. In the absence of noise, the smaller $\|K\|$, the smaller $\|K_{\text{opt}}\|$ (see formula (51)) and thus the smaller the number of terms N required for a given accuracy because the series converges faster.

Step 1 above is a common step. From equation (11), we see indeed that u_∞ is simply the result of applying the filtered backprojection reconstruction formula of Tretiak and Metz [6] to the available projections. To obtain u_∞, it is needed to first filter the projections $g_0(\phi, s)$ to get

$$g_F(\phi, s) = \int_{|\sigma| \geqslant \overline{\mu}_0} \mathrm{d}\sigma\, |\sigma|\, \mathrm{e}^{\mathrm{i}\, 2\pi\, \sigma\, s}\, \mathcal{F} g_0(\phi, \sigma), \qquad \phi \in [0, \pi). \tag{55}$$

Once $g_F(\phi, s)$ is known, the value of u_∞ at a given point (x, y) is obtained by backprojection according to the equation

$$u_\infty(x, y) = \int_0^\pi \mathrm{d}\phi\, \mathrm{e}^{-\mu_0(-x \sin\phi + y \cos\phi)}\, g_F(\phi, s = x \cos\phi + y \sin\phi). \tag{56}$$

Since we are only interested in computing $f_0 = \chi\, u_\infty$, equation (56) only needs to be implemented for pixels inside Ω. (Pixels outside Ω are not of interest since $\chi(\underline{x}) = 0$ if $\underline{x} \notin \Omega$.) The number of operations required to compute f_0 on a grid of $(2\,Q + 1) \times (2\,Q + 1)$ pixels from $2\,Q + 1$ projections is $\mathrm{O}(Q^3)$.

Step 2 requires a method to compute the action of K on a given image ψ and also a method to compute $\|K\|$ from which γ_{opt} is defined (equation (50)). First, we explain how to compute $K\psi = \chi\,(w_\infty * \chi\psi)$ for a given ψ. Consider that $\chi\psi$ is known on the grid of points

$$(x_k, y_l) = (kd, ld), \qquad k, l = -Q, \ldots, Q, \tag{57}$$

covering Ω with $d = D/Q$. To compute $K\psi$, we use the discrete convolution formula

$$(w_\infty * \chi\psi)(x_k, y_l) \simeq d^2 \sum_{k'=-Q}^{Q} \sum_{l'=-Q}^{Q} w_b\big((k-k')\,d, (l-l')d\big)\,(\chi\psi)(x_{k'}, y_{l'}),$$
$$k, l = -Q, \ldots, Q, \tag{58}$$

where w_b is a regularized version of w_∞ defined below. After zeroing out the pixels which are outside Ω, this formula provides an estimate of $K\psi$.

The regularization of w_∞ in (58) is required because w_∞ is singular along the line $x = 0$. The definition of w_b is based on a modified expression of formula (12) for w_∞. Namely,

$$\begin{aligned} w_\infty(x, y) &= \frac{\sinh \mu_0 y}{\pi y}\, h(x) - \int_{-1}^{1} \mathrm{d}p\, \mathrm{e}^{\mu_0 p y} \int_{|\sigma| \leqslant \overline{\mu}_0 |p|} \mathrm{d}\sigma\, \mathrm{i}\, \overline{\mu}_0\, \mathrm{sign}(\sigma)\, \mathrm{e}^{\mathrm{i}\,2\pi\, x\sigma} \\ &= \frac{\sinh \mu_0 y}{\pi y}\, h(x) + \frac{\overline{\mu}_0}{\pi\, x} \left\{ \frac{2 \sinh \mu_0 y}{\mu_0 y} - \frac{\sinh \mu_0 (y + \mathrm{i}x)}{\mu_0 (y + \mathrm{i}x)} - \frac{\sinh \mu_0 (y - \mathrm{i}x)}{\mu_0 (y - \mathrm{i}x)} \right\} \end{aligned} \tag{59}$$

where

$$h(x) = \int_{\mathbb{R}} \mathrm{d}\sigma\, \mathrm{i}\, \mathrm{sign}(\sigma)\, \mathrm{e}^{\mathrm{i}2\pi x\sigma} \tag{60}$$

is the convolution kernel of the Hilbert transform. We replace $h(x)$ in (59) by

$$h_b(x) = \int_{|\sigma| < b} \mathrm{d}\sigma\, \mathrm{i}\, \mathrm{sign}(\sigma)\, \mathrm{e}^{\mathrm{i}2\pi x\sigma} = \frac{\cos(2\pi x b) - 1}{\pi x} \tag{61}$$

with $b = 1/2d$ equal to the Nyquist frequency corresponding to the image sampling. This modifies w_∞ into the smooth function

$$w_b(x, y) = \frac{\sinh \mu_0 y}{\pi y}\, h_b(x) + \frac{\overline{\mu}_0}{\pi\, x} \left\{ \frac{2 \sinh \mu_0 y}{\mu_0 y} - \frac{\sinh \mu_0 (y + \mathrm{i}x)}{\mu_0 (y + \mathrm{i}x)} - \frac{\sinh \mu_0 (y - \mathrm{i}x)}{\mu_0 (y - \mathrm{i}x)} \right\}. \tag{62}$$

By using a 2D fast Fourier transform algorithm for the computation of the discrete convolution (58), the number of operations required for the application of K to a given image is $\mathrm{O}(Q^2 \log Q)$.

Now, we explain how to estimate the norm of K. The idea is simply to use the power method for the computation of the maximum eigenvalue of $K^* K$ where $K^* = -K$ is the adjoint operator of K. The square root of this eigenvalue is mathematically equal to $\|K\|$. Using the power method, $\|K\|$ is found as the limit of the sequence β_l generated through the iterative steps

$$z_l = K\psi_{l-1}, \qquad y_l = -Kz_l, \qquad \beta_l = \|z_l\|, \quad \psi_l = y_l/\|y_l\|, \qquad l = 1, 2, 3, \ldots \tag{63}$$

where ψ_0 is an arbitrary non-zero image (see [26] for more details). In these steps, the application of K to the images ψ_{l-1} and z_l is performed using equation (58). Note that a high accuracy is not required on $\|K\|$. Therefore, only a few iterations are needed.

Step 3 is trivial and can be performed in $\mathrm{O}(N\,Q^2)$ operations, so that the total number of operations required for the computation of f_N is $\mathrm{O}(Q^3)$ as long as $N \ll Q$. This number is similar to the number of operations required for the reconstruction from data on 360°.

The reconstruction formula (53) was tested on simulated data of a simplified head phantom consisting of three ellipses. Table 1 gives a description of that phantom. The attenuation factor used to generate the data was $\mu_0 = 0.012\ \text{mm}^{-1}$. This value corresponds to tissue attenuation. Three reconstructions were performed on a grid of 128×128 pixels of side 2 mm. In each case, there were 128 rays per projection with a sampling distance $\Delta s = 2$ mm.

Table 1. Definition of the ellipses forming the simplified head phantom.

Ellipse	Centre (mm)	Major axis (mm)	Minor axis (mm)	Activity
I	(0, 0)	105	90	680
II	(0, 40)	45	25	480
III	(−35, −45)	27.5	27.5	230

The first reconstruction is shown in the first row of figure 3. This result was obtained from 256 projections sampled on 360° using the filtered backprojection algorithm of Tretiak and Metz [6]. The reconstruction is very accurate since the data were finely sampled over 360° and the method relies on an exact formula linking $f(\underline{x})$ to $g_0(\phi, s)$ with $\phi \in [0, 2\pi)$.

The second reconstruction, shown in the second row of figure 3, is the image χu_∞. This reconstruction was obtained from 256 projections sampled on 180°. The result is very inaccurate and shows that the projections are really required to be known over 360° to obtain good results with the filtered backprojection method of Tretiak and Metz.

The third row of figure 3 shows the sum of the first 15 terms in the series (53). It was computed that $\|K\| = 1.1055$. So, convergence of the series was not ensured without relaxation. The modified operator $\hat{K}_{\text{opt}}$ had a norm $\|\hat{K}_{\text{opt}}\| = 0.74$. In this case, the reconstruction using 15 terms was found to be as accurate as the Tretiak and Metz result of the first row, while using only data on 180°.

5. Conclusion

In this paper, we have shown that stable and exact reconstruction in 2D SPECT imaging does not require the data to be known over 360° as has been previously assumed. A range of 180° was shown to be sufficient when the activity is contained in a convex region where the attenuation is constant. A reconstruction algorithm using only data on a half-turn was also given. This algorithm is as efficient as the FBP algorithm of Tretiak and Metz [6] but may not be optimally designed to handle data noise. Further work is required to compare the performance of the method with alternative techniques using data on 360°.

Appendix

In this section, we show that the sequence $K_n\psi = \chi\ (w_n * \chi\ \psi)$ converges in $L^2(\Omega)$ for any function $\psi \in L^2(\Omega)$, where w_n is defined by equation (9). To prove this result, we write $K_n\psi$ in the form

$$K_n\psi = K_n^{(1)}\psi - K_n^{(2)}\psi - K_n^{(3)}\psi \tag{64}$$

with

$$K_n^{(l)}\psi = \chi\ (w_n^{(l)} * \chi\ \psi), \qquad l = 1, 2, 3, \tag{65}$$

where

$$w_n^{(1)}(x, y) = \int_{-1}^{1} \mathrm{d}p\, \mathrm{e}^{\mu_0 py} \int_{|\sigma| \leqslant \sqrt{n^2+\overline{\mu}_0^2}} \mathrm{d}\sigma\, \mathrm{i}\, \overline{\mu}_0\, \mathrm{sign}(\sigma)\, \mathrm{e}^{\mathrm{i}\,2\pi\, x\sigma}, \tag{66}$$

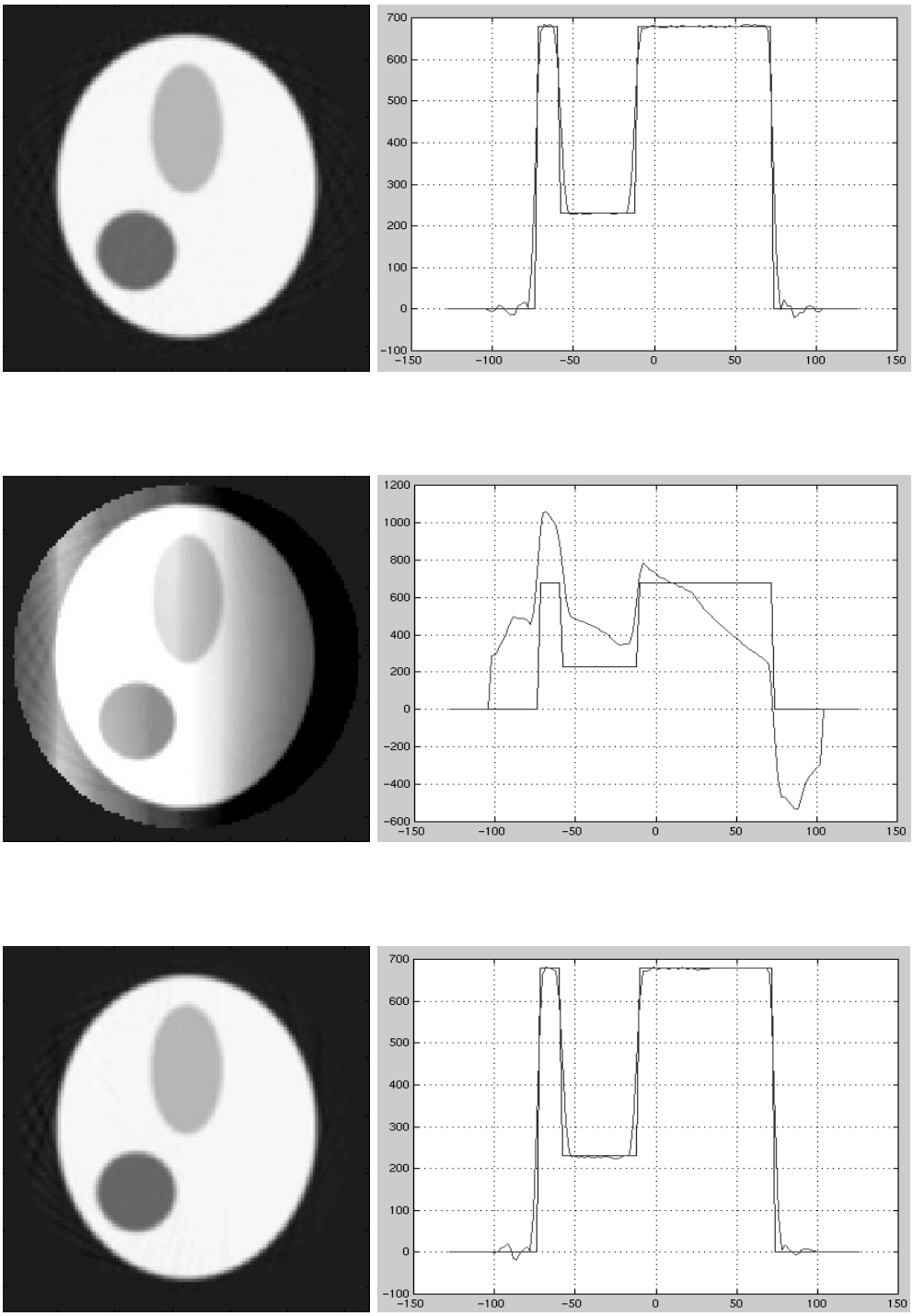

Figure 3. First row: FBP reconstruction from data on 360°. Second row: FBP reconstruction from data on 180° (this image is $\chi\, u_\infty$). Last row: reconstruction using 15 terms of the Neumann series (53). The profiles correspond to the slice $y = 60$ mm. The attenuation factor was $\mu_0 = 0.012\ \text{mm}^{-1}$.

$$w_n^{(2)}(x, y) = \int_{-1}^{1} \mathrm{d}p\, \mathrm{e}^{\mu_0 p y} \int_{\sqrt{n^2+\overline{\mu}_0^2\, p^2} \leqslant |\sigma| \leqslant \sqrt{n^2+\overline{\mu}_0^2}} \mathrm{d}\sigma\, \mathrm{i}\, \overline{\mu}_0\, \mathrm{sign}(\sigma)\, \mathrm{e}^{\mathrm{i}\, 2\pi\, x\sigma}, \tag{67}$$

and

$$w_n^{(3)}(x, y) = \int_{-1}^{1} \mathrm{d}p\, \mathrm{e}^{\mu_0 p y} \int_{|\sigma| \leqslant \overline{\mu}_0\, |p|} \mathrm{d}\sigma\, \mathrm{i}\, \overline{\mu}_0\, \mathrm{sign}(\sigma)\, \mathrm{e}^{\mathrm{i}\, 2\pi\, x\sigma}. \tag{68}$$

Then, we show that each sequence $K_n^{(l)}\psi$ converges individually in $L^2(\Omega)$.

The sequence $K_n^{(1)}\psi$ is first considered. Note that $w_n^{(1)}(x, y) = \rho(y)\, h_n(x)$ with

$$\rho(y) = \frac{\sinh \mu_0 y}{\pi y} \tag{69}$$

and

$$h_n(x) = \int_{\mathbb{R}} \mathrm{d}\sigma\, \mathrm{i}\, \mathrm{sign}(\sigma)\, \chi_n(\sigma)\, \mathrm{e}^{\mathrm{i}2\pi\sigma x}, \tag{70}$$

where

$$\chi_n(\sigma) = \begin{cases} 1 & \text{if} \quad \sigma^2 < n^2 + \overline{\mu}_0^2 \\ 0 & \text{otherwise.} \end{cases} \tag{71}$$

Let

$$\tilde{\rho}(y) = \begin{cases} \rho(y) & \text{if} \quad |y| < 2D \\ 0 & \text{otherwise.} \end{cases} \tag{72}$$

By definition,

$$\begin{aligned} (K_n^{(1)}\psi)(x, y) &= \chi(x, y) \int_{-\infty}^{\infty} \mathrm{d}y'\, \rho(y - y') \int_{-\infty}^{\infty} \mathrm{d}x'\, h_n(x - x')\, \psi(x', y')\, \chi(x', y') \\ &= \chi(x, y) \int_{-\infty}^{\infty} \mathrm{d}y'\, \tilde{\rho}(y - y') \int_{-\infty}^{\infty} \mathrm{d}x'\, h_n(x - x')\, \psi(x', y')\, \chi(x', y'). \end{aligned} \tag{73}$$

Since $\tilde{\rho}\, h_n$ and $\chi\, \psi$ are both in $L^2(\mathbb{R}^2)$, the relation of Parseval can be applied to obtain

$$\begin{aligned} (K_n^{(1)}\psi)(x, y) &= \chi(x, y) \int_{-\infty}^{\infty} \mathrm{d}X \int_{-\infty}^{\infty} \mathrm{d}Y\, (\mathcal{F}\tilde{\rho})(Y) \\ &\quad \times \mathrm{i}\, \mathrm{sign}(X)\, \chi_n(X)\, (\mathcal{F}(\chi\, \psi))(X, Y)\, \mathrm{e}^{\mathrm{i}2\pi(xX+yY)} \\ &= \chi(x, y) \int_{-\infty}^{\infty} \mathrm{d}X \int_{-\infty}^{\infty} \mathrm{d}Y\, \eta_n(X, Y)\, \mathrm{e}^{\mathrm{i}2\pi(xX+yY)} \end{aligned} \tag{74}$$

with $\eta_n(X, Y) = \mathrm{i}\, \mathrm{sign}(X)\, \chi_n(X)\, (\mathcal{F}\tilde{\rho})(Y)\, (\mathcal{F}(\chi\, \psi))(X, Y)$. Now, observe that $\eta_n(X, Y) \in L^1(\mathbb{R}^2)$ as is any product of two functions in $L^2(\mathbb{R}^2)$ and observe also that $\eta_n(X, Y) \in L^2(\mathbb{R}^2)$ because $\mathcal{F}(\chi\, \psi) \in L^2(\mathbb{R}^2)$ and $\mathcal{F}\tilde{\rho}$ is bounded since $\tilde{\rho} \in L^1(\mathbb{R})$. Therefore, $\mathcal{F}\eta_n \in L^2(\mathbb{R}^2)$ and $K_n^{(1)}\psi \in L^2(\Omega)$ with

$$\|K_p^{(1)}\psi - K_q^{(1)}\psi\|^2 \leqslant \|\mathcal{F}\eta_p - \mathcal{F}\eta_q\|^2 \leqslant \|\eta_p - \eta_q\|^2 \tag{75}$$

which tends to zero when p and q tend to ∞. Thus, $K_n^{(1)}\psi$ converges in $L^2(\Omega)$.

Now, the sequence $K_n^{(2)}\psi$ is considered. It is easy to see that $w_n^{(2)}(x, y)$ is a continuous function and that

$$|w_n^{(2)}(x, y)| \leqslant 2\, \overline{\mu}_0^3\, \mathrm{e}^{\mu_0 |y|}\, \frac{1}{n + \sqrt{n^2 + \overline{\mu}_0^2}}. \tag{76}$$

Therefore,

$$|(K_n^{(2)}\psi)(x,y)| \leqslant \chi(x,y)\, 2\,\overline{\mu}_0^3\, \mathrm{e}^{2\mu_0 D}\, \frac{1}{n+\sqrt{n^2+\overline{\mu}_0^2}} \int_{-\infty}^{\infty}\int_{-\infty}^{\infty} \mathrm{d}x'\,\mathrm{d}y'\,|(\chi\,\psi)(x',y')|. \quad (77)$$

Thus, $K_n^{(2)}\psi$ converges to zero in $L^2(\Omega)$.

Finally, consider the sequence $K_n^{(3)}\psi$. This sequence is constant, so it is sufficient to show that $K_n^{(3)}\psi \in L^2(\Omega)$. By definition, $w_n^{(3)}(x,y)$ is a continuous function. Therefore,

$$|(K_n^{(3)}\psi)(x,y)| \leqslant \chi(x,y)\Big(\sup_{\underline{x}\in\Omega,\,\underline{x}'\in\Omega} |w_n^{(3)}(\underline{x}-\underline{x}')|\Big) \int_{-\infty}^{\infty}\int_{-\infty}^{\infty} \mathrm{d}x'\,\mathrm{d}y'\,|(\chi\,\psi)(x',y')|. \quad (78)$$

Thus, $K_n^{(3)}\psi \in L^2(\Omega)$ since it is bounded and supported in Ω.

Acknowledgments

The work of F Noo was supported by the Belgian National Fund for Scientific Research (FNRS, Belgium). The authors would like to thank Michel Defrise from the Free University of Brussels and Frank Natterer from the University of Münster for constructive suggestions. The authors are also thankful to Patricia Comeford for her help in writing the manuscript.

References

[1] Novikov R G 2000 An inversion formula for the attenuated x-ray transformation *Preprint* CNRS, UMR 6629, Departement de mathematiques, Université de Nantes, France
[2] Natterer F 2001 Inversion of the attenuated Radon transform *Inverse Problems* **17** 113–9
[3] Kunyansky L A 2001 A new SPECT reconstruction algorithm based on the Novikov explicit inversion formula *Inverse Problems* **17** 293–306
[4] Markoe A 1984 Fourier inversion of the attenuated x-ray transform *SIAM J. Math. Anal.* **15** 718–22
[5] Bellini S, Piacenti M, Caffario C and Rocca F 1979 Compensation of tissue absorption in emission tomography *IEEE Trans. Acoust. Speech Signal Processing* **27** 213–8
[6] Tretiak O and Metz C 1980 The exponential Radon transform *SIAM J. Appl. Math.* **39** 341–54
[7] Clough A and Barrett H H 1980 Attenuated Radon and Abel transforms *J. Opt. Soc. Am.* **39** 341–54
[8] Gullberg G T and Budinger T F 1981 The use of filtering methods to compensate for constant attenuation in single-photon emission computed tomography *IEEE Trans. Biomed. Eng.* **8** 142–57
[9] Finch D V and Hertle A 1987 The exponential Radon transform *Intregral Geometry (Contemporary Mathematics, vol 63)* ed Bryant, Guillemin, Helgason and Wells (Providence, RI: American Mathematical Society) pp 67–73
[10] Hawkins W G, Leichner P K and Yang N C 1988 The circular harmonic transform for SPECT reconstruction and boundary conditions on the Fourier transform of the sinogram *IEEE Trans. Med. Imaging* **7** 135–48
[11] Inouye T, Kose K and Hasegawa A 1989 Image reconstruction algorithm for single-photon-emission computed tomography with uniform attenuation *Phys. Med. Biol.* **34** 299–304
[12] Hazou I A and Solmon D C 1988 Inversion of the exponential x-ray transform. I: analysis *Math. Methods Appl. Sci.* **10** 561–74
[13] Hazou I A and Solmon D C 1989 Filtered-backprojection and the exponential Radon transform *J. Math. Anal. Appl.* **141** 109–19
[14] Hazou I A and Solmon D C 1990 Inversion of the exponential x-ray transform. II: numerics *Math. Methods Appl. Sci.* **13** 205–18
[15] Gullberg G T and Zeng G L 1994 Reconstruction algorithm using singular value decomposition of a discrete representation of the exponential Radon transform using natural pixels *IEEE Trans. Nucl. Sci.* **41** 2812–9
[16] Liang Z, Ye J and Harrington D P 1994 An analytical approach to quantitative reconstruction of non-uniform attenuated brain SPECT *Phys. Med. Biol.* **39** 2023–41
[17] Metz C E and Pan X 1995 A unified analysis of exact methods of inverting the 2D exponential Radon transform, with implications for noise control in SPECT *IEEE Trans. Med. Imaging* **14**
[18] Pan X and Metz C E 1995 Analysis of noise properties of a class of exact methods of inverting the 2D exponential Radon transform *IEEE Trans. Med. Imaging* **14**

[19] Liang Z, Ye J, Cheng J and Harrington D P 1996 The inversion of the exponential Radon transform for quantitative brain SPECT *Phys. Med. Biol.* **41** 1227–32
[20] Weng Y, Zeng L and Gullberg G T 1997 Analytical Inversion formula for uniformly attenuated fan-beam projections *IEEE Trans. Nucl. Sci.* **44** 243–9
[21] You J, Liang Z and Zeng G L 1999 A unified reconstruction framework for both parallel-beam and variable focal-length fan-beam collimators by a Cormack-type inversion of exponential Radon transform *IEEE Trans. Med. Imaging* **18** 59–65
[22] Clarkson E 1999 Projections onto the range of the exponential Radon transform and reconstruction algorithms *Inverse Problems* **15** 563–71
[23] Kuchment P and Shneiberg I 1994 Some inversion formulae in the single photon emission computed tomography *Appl. Anal.* **53** 221–31
[24] Palamodov V P 1996 An inversion method for an attenuated x-ray transform *Inverse Problems* **12** 717–29
[25] Kreyszig E 1989 *Introductory Functional Analysis with Applications* (New York: Wiley)
[26] Johnson L W and Riess R D 1977 *Numerical Analysis* (Reading, MA: Addison-Wesley)